



A scalable laser system at 461 nm for laser cooling and trapping of Sr atoms

Gunjan Verma^{1,2} · Enlong Wang¹ · Joep Assendelft¹ · Nicola Poli^{1,3} · Gabriele Rosi¹ · Guglielmo Maria Tino¹ · Leonardo Salvi¹

Received: 14 February 2022 / Accepted: 6 April 2022 / Published online: 16 May 2022
© The Author(s) 2022, corrected publication 2022

Abstract

The realization of compact high-power narrow-linewidth laser sources in the visible range has been a long-standing interest for the atomic physics community, especially in the field of laser cooling and trapping of alkaline-earth and alkaline-earth-like atoms. We report a simple master-slave injection-locked laser system capable of generating 500 mW at 460.86 nm with a linewidth of 1.6 MHz to realize magneto-optical trapping of strontium atoms on the $5s^2 \ ^1S_0 - 5s5p \ ^1P_1$ transition. The master laser used is an external cavity diode laser built with an anti-reflection coated laser diode in a Littrow configuration and the slave laser is built with a recently launched single mode high power GaN laser diode. We characterized the frequency noise, injection stability, spectral purity and relative intensity noise of the laser system. The reported laser system is used routinely to produce 10^7 strontium atoms at a temperature of 10 mK in a magneto-optical trap. The laser system offers a prominent alternative to the existing frequency-doubled laser systems in terms of cost, design flexibility, electrical power consumption, ease of scaling, intensity stability, and frequency tunability. The proposed system is also an effective solution for space-based experiments where a laser system's size, weight, and electrical power consumption are crucial design parameters.

1 Introduction

Low-noise, high-power tunable laser sources are a fundamental and inevitable tool for the atomic physics community where a search for simple, easy to maintain, portable, and stable, compact laser systems has always been desired [1, 2]. The realization of laser sources led to the advent of ultracold atoms which in turn advanced various fields varying from high precision metrology [3–6] to quantum simulations [7]. For the new generation of frequency standards and atom interferometers, alkaline-earth atoms and alkaline-earth-like atoms such as Yb [8, 9], Ca [10], Sr [11], Hg [12], Mg [13] and Cd [14] have been considered as interesting species.

These atoms are being actively studied due to the presence of peculiar features such as the presence of intercombination transitions that allow to reach ultra-low temperatures [15] and to realize optical lattice clocks [16]. Among these atoms, in recent years, Sr has gained considerable attention and not only allowed the realization of high precision optical clocks [17, 18], atom interferometers [19, 20] but opened the prospects of using it for gravitational wave detection [21] and dark matter exploration [22, 23]. Strontium is also being considered as a promising candidate for space-based experiments [24–26] and many other experiments involving the investigation of spin gravity couplings [27], standard model extensions [28] and dilaton models [29]. With a high interest in Sr, we continue to see efforts from the community in finding innovative and efficient methods to realize ultracold samples of Sr atoms [30, 31].

One of the challenges in addressing the laser cooling and trapping of the atoms mentioned above is the realization of compact, high-power, narrow-linewidth, single-mode stable laser sources in the visible (violet-blue region) range. Demand for stable laser sources in this wavelength range is not only limited to the cooling and trapping of the atoms mentioned earlier [32–34]. Often, such laser sources are not readily available and implemented using frequency

Gunjan Verma and Enlong Wang contributed equally to this work.

✉ Leonardo Salvi
leonardo.salvi@unifi.it

¹ Dipartimento di Fisica e Astronomia and LENS-Università di Firenze, INFN-Sezione di Firenze, Via Sansone 1, 50019 Sesto Fiorentino, Italy

² Dipartimento di Matematica e Informatica ‘Ulisse Dini’, Università di Firenze, Firenze, Italy

³ CNR-INO, Firenze, Italy

conversion systems [14, 35–37]. While being complex, expensive and possibly requiring high maintenance, these options often imply aging effects [38, 39] and moderate-intensity noise [40, 41].

Thus, systems that can produce light directly from laser diodes may be preferable and are currently being implemented in some experiments. In the particular case of high-power laser systems at ≈ 461 nm, efforts have been taken to build these sources using single-mode diode lasers in combination with an amplifier chip in the master oscillator power amplifier (MOPA) configuration [42, 43]. However, these systems are yet to become commercially available. Besides the amplifier chip-based laser systems, optical-injection locked (OIL) laser systems [44] where a high-power laser (slave) is injected with a weaker well stabilized single-mode laser (master) are also being explored actively [41, 45, 46]. Injection locking [47] is a promising technique used for transferring the spectral purity of a master to a slave [48].

The power enhancement of an injection-locked system can be higher than if the same laser medium is operated as a linear amplifier (i.e., MOPA source). In previous studies, the required level of optical power (≈ 300 mW) at 461 nm in Sr experiments was derived using multiple slave lasers [49] in contrast to our system where we use a single diode to derive 500 mW of optical power. Low-power, manual injection locking of the slave, and poor fiber coupling efficiency limited the performance of earlier reported systems. Some recent studies have addressed the problem of manual injection locking by designing the injection locking schemes based on monitoring a Fabry-Perot (FP) cavity transmission [50]. A detailed study of such a laser system's performance and lifetime is required as few experiments have adopted this relatively new technology in the violet-blue region. We point out that no reported results exist, to our knowledge, on the achievement of a magneto-optical-trap (MOT) with a single slave laser diode.

In this paper, we report a master-slave-based, narrow-linewidth (1.6 ± 0.6 MHz above 1 kHz) laser system capable of delivering ≈ 500 mW power at 460.86 nm with a relative intensity noise level of -124.5 dBc/Hz above 1 kHz. The slave diode used in our system is a recently launched single mode high power GaN laser diode (Nichia NDV4B16 [46, 51]). This laser diode features a peak wavelength of 458 nm and maximum output power of ≈ 500 mW. In literature, we found two recent papers which mentioned working with the same diode [45, 52]. In Ref. [52], the paper discusses the use of diode for upgrading the power of a Zeeman slower beam in their experiment. In Ref. [45], the authors presented the diode's characterization and proposed to use it for the laser cooling and trapping of Sr. However the work does not present any information on the injection stability, relative intensity noise and frequency instability which are crucial parameters for the realization of a blue MOT. Experiments

involving multiple injection-based systems such as those with limited master laser power or experiments with numerous atomic species would require robust injection locking schemes to avoid frequent manual injection of the slave during the experiment. However, the papers mentioned above do not discuss any active stabilization of the injection. Here, our work attempts to bridge this information gap with a systematic study of the system and adds to the previous work.

Section 2 presents a detailed description of the complete laser system and an active stabilization scheme for the injection locking. In section 3, we characterize the slave injection and discuss the performance of the laser system in the context of spectral purity, frequency tunability, and intensity noise. In Sect. 4, we demonstrate the capability of this laser system in realizing the first-stage cooling of Sr atoms on the $5s^2^1S_0 - 5s5p^1P_1$ transition (natural linewidth, $\Gamma = 2\pi \times 30.5$ MHz). In Sect. 5, we provide our conclusions and discuss future prospects.

2 Laser system

In this section, we describe the complete laser system used to derive various optical beams for spectroscopy, laser cooling, and probing of Sr atoms. The left panel of Fig. 1 shows the optical layout of an injection-locked laser system consisting of a master laser stabilized to a spectroscopic signal and a slave laser to derive light for cooling and trapping. A portion of the master laser output goes to the spectroscopy cell and another is fed into the slave as seed for the injection. The slave output is split into two parts to provide light for the Zeeman slower, MOT, probe and injection monitoring. The master laser is an external cavity diode laser (ECDL) system built in the Littrow configuration [53] using an anti-reflection coated laser diode (LD) (Nichia NDBA116T), an aspheric lens (Thorlabs C230TMD-A) and a holographic grating (Thorlabs GH13-18V). A thermistor (TDK B57861S0103F045) embedded in the laser diode holder monitors the diode temperature, a piezoelectric transducer (PZT) (Thorlabs AE0203D08F) attached to the grating is used to tune the wavelength of the laser, and a Peltier cooler (ETH-127-10-13-S-RS [51]) is used to tune the diode temperature. These components are housed in a closed aluminum box ($W \times L \times H$: $78 \times 109 \times 72$ mm) to make the laser robust against air currents and temperature fluctuations. The LD is oriented so that the polarization of the light remains parallel to the grooves of the grating. The position of the collimating lens is optimized and fixed to reach a minimum lasing threshold current of 103 mA when the laser is operated at 460.862 nm and temperature stabilized at 19.5 °C. To drive and stabilize the ECDL, we use a home-built low noise current and temperature controller. The current controller has two channels; one of the channels

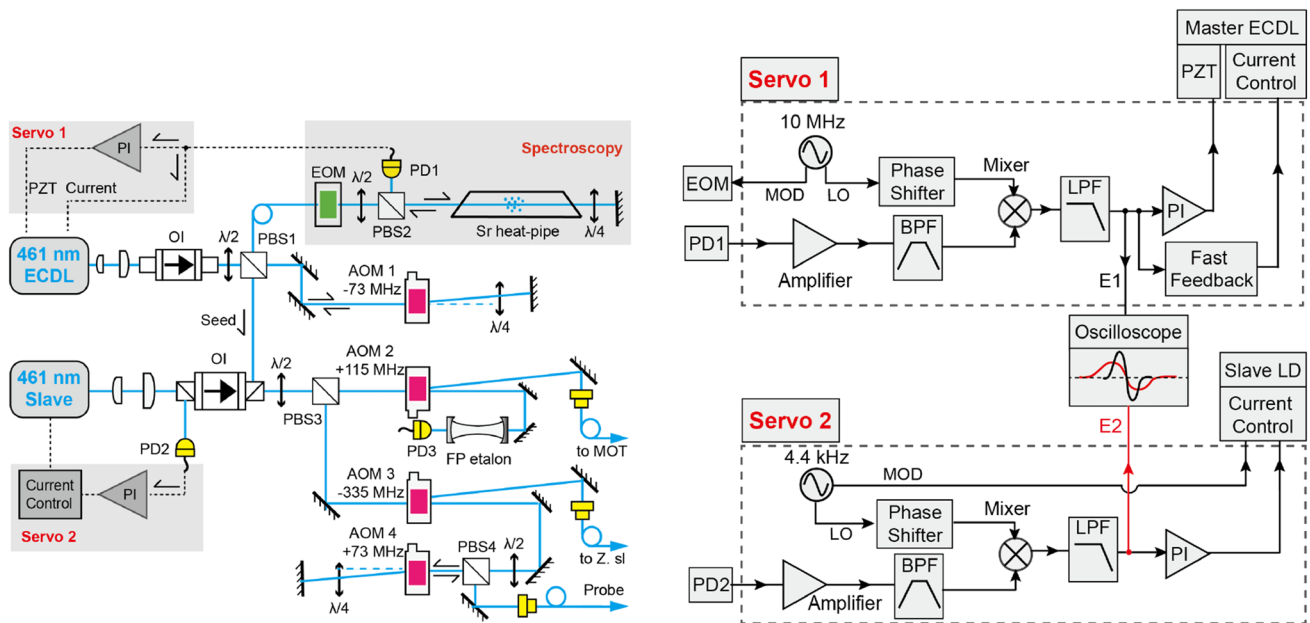


Fig. 1 Laser system: The left panel shows the optical layout with the master ECDL frequency stabilized to a spectroscopy signal, the optical injection into the slave laser, and the splitting of the slave output to provide light for cooling and trapping and for probing the atomic ensemble. The right panel shows the scheme to derive error signals

for active stabilization of the master (servo 1) and the slave injection (servo 2), respectively. Abbreviations: PBS, polarizing beamsplitter; AOM, acousto-optic modulator; EOM, electro-optic modulator; OI, optical isolator; PD, photodetector; PI, proportional-integral controller; Z.sl, Zeeman slower; BPF, band pass filter; LPF, low pass filter

provides stable DC current to the diode. Another channel is used to apply small, sinusoidal modulation to the DC setpoint. We observe a mode hop free tuning range of 7.1 GHz at 460.862 nm. The ECDL delivers ≈ 30 mW of optical power when operated at 155 mA. The beam ellipticity and astigmatism are corrected through a combination of cylindrical lenses ($f = 100$ mm and $f = 30$ mm). After beam shaping, the output of the ECDL is directed through a 30 dB optical isolator and then split into two parts: (a) the first part is used for slave injection, (b) the second part is used for laser frequency stabilization. The frequency of the spectroscopy part is shifted by +146 MHz through a double pass in an AOM (AOM1). A spectroscopy cell is used to stabilize the frequency of the master laser 146 MHz below the $5s^2^1S_0-5s5p^1P_1$ transition. This frequency shift keeps the laser output off-resonant, avoiding the heating and atom loss from the MOT due to scattered light reaching the atoms from the laser system. The shift of the laser output is achieved in a double pass configuration (AOM1) to decouple the beam pointing from the frequency shift, which is required if we need to address the cooling of other isotopes of Sr atoms. The spectroscopy beam is coupled to a polarization-maintaining (PM) fiber, which delivers nearly $600 \mu\text{W}$ of power to an independent small optical board hosting the Sr spectroscopy cell.

The slave laser used in our system is a high-power GaN laser diode (Nichia NDB4916E [51]). We realized the slave laser in a similar aluminum enclosure as the master, the only

difference being the absence of a grating and the PZT in the system. The slave diode is mounted, and the temperature is stabilized in the same manner as the ECDL. An aspheric lens is used to collimate the laser diode output. The collimated elliptical mode of the slave (1:3 aspect ratio) is shaped into a nearly circular beam with a pair of cylindrical lenses ($f = 100$ mm and $f = 30$ mm). The injection/seed beam from the master laser is fed back to the slave through the side port of the optical isolator as shown in the left panel of Fig. 1. The output of the slave is passed through an optical isolator (OI) and then divided into two parts. The first part is passed through AOM2, where the first order shifts the frequency by +115 MHz and is coupled to a PM fiber with 65% coupling efficiency. The output of this fiber is sent to the optical table hosting the vacuum system to prepare the MOT beams, while the zeroth order is coupled to a scanning FP cavity to monitor the slave injection. The +115 MHz shift by AOM2 keeps the MOT beams ~ -30 MHz detuned from the $5s^2^1S_0-5s5p^1P_1$ transition, which is experimentally found to be the optimal detuning for trapping strontium atoms. We monitor the quality of slave injection by detecting the transmission of the scanning Fabry-Perot (FP) cavity with a photodetector (PD3). Single-mode emission is attained by fine tuning the laser's injection current. Nearly 22 mW power is used for preparing the MOT beams. The second part of the slave is sent through AOM3, where the first diffraction order shifts the laser frequency by -335 MHz and is coupled to a PM

fiber which is used for Zeeman slowing of the atomic beam. The -335 MHz shift is decided by the design of our Zeeman slower and the MOT capture velocity, which requires the Zeeman slowing beam to be -481 MHz detuned from the $5s^2\ ^1S_0-5s5p\ ^1P_1$ transition for the effective slowing of the atomic beam. The zeroth-order provides a probe beam used to image the cold atomic cloud. The beam is passed through AOM4 in a double pass configuration to shift the frequency by $+146$ MHz to reach the resonance of the $^1S_0-^1P_1$ transition. All the specific frequency shifts are also chosen to avoid overlapping with other frequencies in the apparatus.

The current required for stable injection may change over time due to the drift in the temperature of the slave diode and the alignment of the injection beam. To get rid of the frequent user intervention for the injection locking and to use a low seed power, we realized a feedback loop (servo 2) as shown in the right panel of Fig. 1 for active stabilization of injection. This scheme was previously used to increase the mode hop free tuning range of an ECDL and then it was implemented to stabilize the slave injection as discussed in Ref. [54, 55]. The error signal for injection locking is derived by modulating the slave current at 4.4 kHz and measuring the intensity noise of the slave with a 100 kHz bandwidth photodetector (PD2). By comparing the phase of the induced amplitude noise with the phase of the sinusoidal drive signal using a low-cost homebuilt lock-in amplifier, an error signal is derived and fed to a PI unit. The output of the PI unit acts on the slave current. In the lock-in amplifier unit, the PD signal is amplified and filtered using a narrow band-pass filter (bandwidth 100 Hz, center frequency 4.4 kHz) and fed to a mixer along with the reference signal (LO). The output of the mixer is sent to a low pass filter to derive the error signal. The error signal is used to lock the slave at the optimum current point by adjusting the DC offset. The working principle of the slave stabilization feedback loop can be understood in the following manner. The current modulation changes the carrier density and temperature of the laser diode, affecting the index of refraction and optical path length of the slave diode allowing for the internal cavity modes of the laser diode to shift. When the slave laser cavity supports an integer number of half-wavelengths of the seeding master, injection locking is attained. This condition is maintained by adjusting the diode's internal cavity optical path length through the slave current. With the feedback applied, the slave can smoothly follow the master during its frequency scanning. For ordinary experiment runs the injection is usually stable over time spans of 5 hours and no active injection stabilization is required in this case. However, for longer experiment runs or when the master is scanned by more than a few hundred MHz, this stabilization method provides an advantage.

The error signal for long-term frequency stabilization of the master laser is produced by phase modulating the

light going to the spectroscopy cell at 10 MHz with an electro-optical modulator (EOM) and demodulating the saturation absorption spectroscopy signal collected by a photodiode (PD1) with a mixer (Minicircuits ZAD-1+ [51]). The spectroscopy cell is a 65 cm-long heat pipe containing Sr in an argon environment. The cell is operated at 260 °C to produce an atomic vapor of Sr atoms in its central region. The ends of the heat pipe are terminated with water-cooled glass windows. The windows are protected against Sr vapor deposition by the argon as it prevents the Sr originating at the center from reaching the ends via collisions. The derived error signal is fed to the laser PZT via a proportional-integral unit (PI) (servo 1) to compensate low-frequency drift of the laser. The PZT can't respond to high-frequency corrections, limiting the bandwidth of the servo. To overcome this, we implement a fast feedback channel acting on the laser current, making the system more robust against vibrations and acoustic noise. The linewidth of the ECDL is estimated to be 1.6 ± 0.6 MHz above a Fourier frequency of 1 kHz without the servo locking, determined from the power spectral density (PSD) of its frequency noise as shown in Fig. 2, using the side-of-fringe method [56]. To measure the frequency noise of the laser, a part of the master laser output is coupled to a temperature-stabilized cavity (finesse ≈ 300 , free spectral range (FSR) ≈ 1.43 GHz). The cavity length is stabilized at half of the cavity resonance transmission peak value. Assuming that cavity length is stable on the time scales of these measurements, fluctuations in the transmission of the cavity around this locking point are

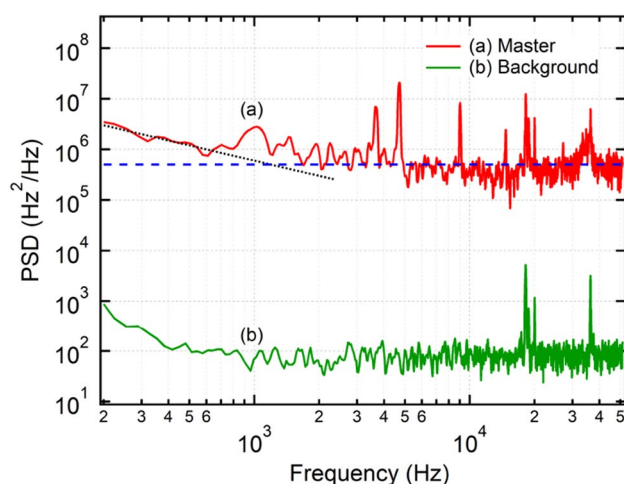


Fig. 2 Frequency noise measurement. The trace (a) shows the frequency noise PSD of the master laser and trace (b) shows the background PSD estimated with a thermal light source incident onto the photodiode. The dashed trace indicates the flat frequency noise level [$S_{f_0}(f) = 0.51 \times 10^6$ Hz²/Hz] above 1 kHz which is used to estimate the lorentzian linewidth of the master laser as $\pi S_{f_0}(f)$. The dotted black trace shows the $1/f$ frequency noise response of the laser

directly proportional to the laser's frequency noise. The intensity noise of the cavity transmission is detected with a silicon PIN photodiode (Hamamatsu S5821-01) based on a low-noise and high-gain transimpedance amplifier photodetector. The photodetector signal is fed to a spectrum analyzer (Agilent 35670A [51]). The current noise of the laser driver is found to be the dominant source for the laser frequency noise which suggests that the laser linewidth can be reduced further with the help of a lower noise laser driver.

We use two independent power supply racks to power the master, slave and the locking electronics. We measured the power consumption of each unit to be nearly 45 W. Therefore the total power consumption of our system is less than 100 W which can be further optimised with better supplies, making it a favourable choice for the space-borne experiments. To draw a comparison, the power consumed by the current and temperature controls as well as the servo amplifier is 8 W.

3 Characterisation and performance of the slave emission

This section describes the characterization of the slave laser as a function of operating current and injection power and compares the spectral purity and intensity noise of the injected slave laser with that of the master laser.

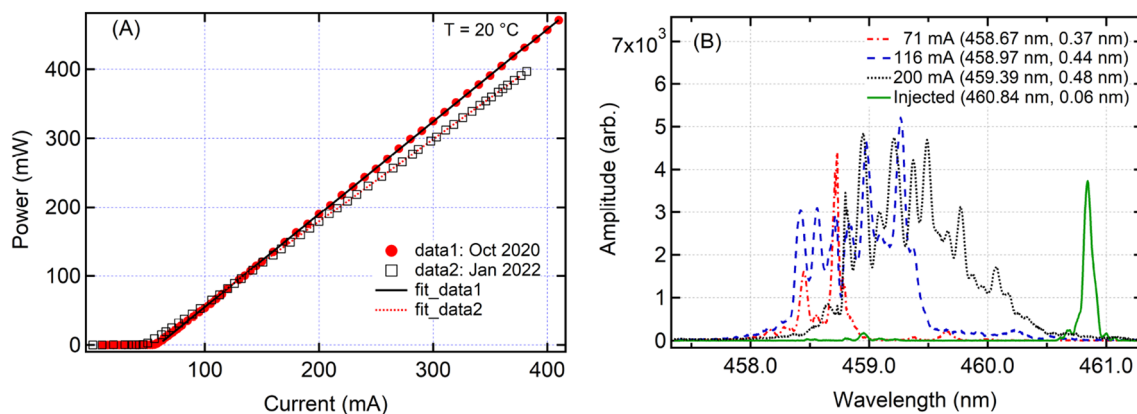


Fig. 3 Main properties of the free-running slave laser. **A** shows the optical power of the slave ($T = 20\text{ }^{\circ}\text{C}$) as a function of current as monitored over a period of roughly one year to observe the aging of the slave laser. The filled circle (red) and the empty square (black) show the data recorded in October 2020 and January 2022 respectively. The solid (black) and dashed (red) line shows the fit (see text) to the respective data. We operate the slave close to 300 mA to get an output of 324 mW for Sr laser cooling and trapping. **B** shows the slave emission spectrum for different operating currents (71–

3.1 Slave injection characterization

The current-power characteristic of the free-running slave diode stabilized at $20\text{ }^{\circ}\text{C}$ is shown in Fig. 3A. The current-power characteristic was remeasured after one year to observe the aging of the diode. The figure shows a threshold current of 59 mA and a $1.346 \pm 0.001\text{ mW/mA}$ slope efficiency above the threshold for the data recorded in October 2020 and a threshold current of 51 mA and a $1.199 \pm 0.001\text{ mW/mA}$ slope efficiency above the threshold for the data recorded in January 2022. A low threshold and linear increase in the current above the threshold even after one year indicate the good working condition of the diode. However, nearly 11% decrease in the slope efficiency over a year would require the operational current of the slave diode to be increased in the subsequent years. We typically operated the slave at 300 mA to derive 324 mW of optical power with an optical injection of 2.4 mW at 460.862 nm for the experiment. The maximum current at which the diode can be operated is 600 mA and given a $\sim 11\%$ decrease in the slope efficiency every year, we infer a lifetime of the diode to be ~ 5 years, assuming that the degradation happen at a constant rate. Figure 3B shows the spectrum of the slave at different operational laser currents, measured through a home-built optical spectrum analyzer based on a diffraction grating. From the measured spectrum, the center wavelength, λ_c and dispersion (width of the emission spectrum), $\Delta\lambda$ can be calculated as

200 mA). The legend indicates the slave operating current, center wavelength, and dispersion of the spectrum. The spectrum shifts towards a higher wavelength for a larger operating current (as shown by dashed-dotted red trace (71 mA), dashed blue trace (116 mA) and dotted black (200 mA) trace in the figure). The solid (green) curve shows the single-mode emission from the injected slave when operated at 200 mA. The dispersion of the injected slave spectrum is limited by the resolution of the spectrometer

$$\lambda_c = \frac{\int \lambda P(\lambda) d\lambda}{\int P(\lambda) d\lambda} \tag{1}$$

$$\Delta\lambda = \sqrt{\frac{\int (\lambda - \lambda_c)^2 P(\lambda) d\lambda}{\int P(\lambda) d\lambda}} \tag{2}$$

where $P(\lambda)$ is the measured distribution. These relations correspond to the usual mean and standard deviation of the measured distribution. At 71 mA, the emission of the diode is observed to be dominant in the 458–459 nm region. At the same time, as it is operated at higher currents, the emission shifts towards higher wavelengths, as expected based on thermal effects. This feature helps us understand the slave behavior where we noticed that for a given seed power (≈ 1.1 mW), it was easier to inject the slave at higher operating currents. The seed power quoted in the paper refers to the power reaching the slave laser output.

When the frequency of an injected signal is tuned to the slave oscillation frequency the overall regenerative gain overtakes the intracavity losses and emission at the master frequency occurs. The electrical power consumption of the laser system can be reduced if the slave diode’s temperature need not be stabilized far from room temperature to attain emission closer to the master emission wavelength. A good spatial mode overlap between the master and the slave can result in the slave injection, which can be easily observed at higher currents above 120 mA. Once the slave is injected, the injection can be further improved by fine-tuning the alignment near the injection point. For a given master frequency, injection can be achieved by adjusting the slave

temperature, current, and injection (seed) power. We were able to achieve the injection by tuning the slave current for seed powers > 0.4 mW.

To understand the behavior of the slave laser and the quality of injection, we looked at the transmission of an optical cavity as shown in the inset of Fig. 4A. The plot shows the transmission of the cavity coupled with the slave output as a function of slave current for two different seed power. Given that the master frequency and cavity length are stable on the time scales of these measurements, the transmission of the cavity as a function of slave current around the injection point indicates a range of slave current for which robust and stable injection locking can be achieved. The slave current is scanned at a rate of 7 Hz with a triangular wave. The current interval, for which the transmission of the cavity remains constant, is referred to as the locking range where stable injection can be achieved. The curve shows an asymmetry about the flat window region, where we observe a gradual drop in the cavity transmission on the high-current side and a rapid decline on the low-current side. This asymmetry may arise from the combination of Joule heating of the laser cavity from diode current and heating from seed light resonance [50] or can be attributed to the linewidth enhancement factor [57]. To obtain stable injection locking, the difference in their frequencies $\Delta\omega$ must lie within the locking range. Typical injection locking ranges are a few nanometers or less. The bounds of this locking range are defined as $\Delta\omega_{\min}$ and $\Delta\omega_{\max}$ given by $\Delta\omega_{\min} = -\kappa\sqrt{1 + \beta^2}\sqrt{P_{\text{inj}}/P_0}$ and $\Delta\omega_{\max} = \kappa\sqrt{P_{\text{inj}}/P_0}$, where P_0 and P_{inj} are the output powers of the slave and the master lasers, respectively, β is the linewidth enhancement

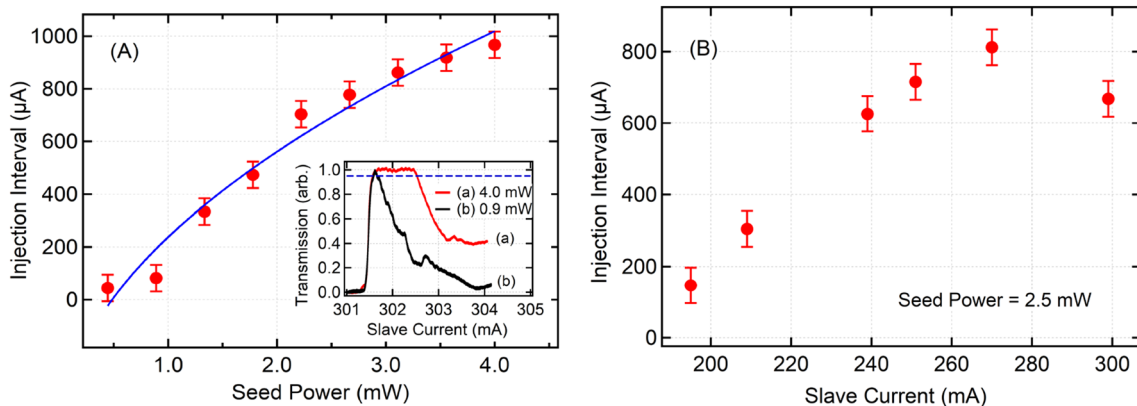


Fig. 4 Slave injection characterization: **A** shows the injection interval (range of slave current around the optimum injection set point (≈ 300 mA) for which the slave remains injected) as a function of seed power. Filled red circles are the data points, and the blue curve expresses the fitting function. Injection interval varies as $A\sqrt{P_{\text{inj}}}$ as discussed in section 3. The inset plot of (A) shows the transmission of a cavity (free spectral range ≈ 1.43 GHz, finesse ≈ 300 @ 461 nm)

coupled with the slave output ($\approx 60 \mu\text{W}$) as a function of the slave current around the injection point for two different seed powers. Curve (a) for 4.0 mW and curve (b) for 0.9 mW. The injection interval is measured as the current interval for which the cavity transmission normalized by the peak power remains above 95%. (B) shows the injection interval as a function of slave current for a given seed power (2.5 mW)

factor which describes the amplitude-phase coupling (a phase change due to changes in the carrier density-dependent refractive index), $\kappa = w_s/2Q$ is the coupling coefficient that describes the rate at which the injected photons enter into the slave diode cavity. w_s is the free-running slave carrier frequency, and Q is the cavity quality factor. It can be seen that for low- Q lasers, the coupling coefficient would be higher and will provide a more extensive locking range and therefore make locking of such lasers easier. However, low Q also leads to increased laser linewidth and reduced phase noise performance of the slave laser. An extreme case of Q tending to zero would be the case of semiconductor optical amplifiers, amplifying any injected signal within the gain region.

A non-zero linewidth enhancement factor can lead to an asymmetric locking range as observed in our data (inset of Fig. 4A). The injection interval is measured as the current interval where the cavity transmission signal remains higher than a threshold value given by 95% of the maximum. While the observed asymmetric feature can be attributed to misalignment of the injection beam [58], it persists in a variety of situations, even for optimized alignment. The data in Fig. 4A, showing the injection interval as a function of seed power, is found to be in quantitative agreement with the predicted behavior where injection interval or locking range increases as $A\sqrt{P_{\text{inj}}}$ where A is estimated to be $782 \pm 124 \mu\text{A}/\sqrt{\text{mW}}$. We also observed hysteresis in the shape of the spectral purity curve. The width of the injection interval is found to be smaller when measured with increasing current and broader when observed with decreasing current. We observe an increase in the injection interval with increasing current and a drop above 270 mA, suggesting the existence of an optimum current value for a given seed power (2.5 mW) as shown in Fig. 4B. During the operation of the slave, we noticed that it could be partially injected until ≈ 80 mA and completely injected above 80 mA with seed powers > 0.4 mW. Regions of stable injection only exist in definite current regions. These regions are spaced by ≈ 20 mA and are ≈ 0.05 – 1 mA wide depending on the seed power or slave current as shown in Fig. 4. The specific location of these intervals depends on the temperature of the slave and the frequency difference between the master and the slave. The width of these modes depends on the operating current and the seed power. The slave can get out of injection in a few minutes if the injection interval is very narrow.

3.2 Scalability and tunability

As shown in Fig. 4A, an injection power of nearly 1 mW is sufficient to inject a single slave laser giving an excess to maximum of 500 mW of optical power. However, a single

master laser can be easily used to inject multiple slaves (at least 6 in our case) simultaneously if one wishes to scale the optical power. We observed that the slave can be tuned over a range of 1.4 GHz with complete injection for a seed power of 2.4 mW. The tunability of the slave reduces as the injection power is reduced which can be compensated with the injection locking.

3.3 Spectral purity

Master-slave beatnote: to quantify the laser system's spectral purity near the central emission peak, we measured the beatnote obtained by combining the master and slave laser beams. We record the beatnote between a reference beam (derived by frequency shifting the master laser by 146 MHz) and the slave laser using a spectrum analyzer (Agilent N9320A). The laser beams with the same polarization were combined on a nonpolarizing beam splitter and focused on an AC coupled 1.2 GHz bandwidth photodetector (ET-2030A [46, 51]). This measurement (master-slave) is compared with a reference measured between the master and the reference beam, while keeping the total power on the photodiode the same in both cases. Ideally, the beatnote between the master and the reference beam (master-master) should look like a delta function at 146 MHz. As shown in the left panel of Fig. 5, however, the beat signal with an offset frequency of 146 MHz has a finite width. The width can be associated with the optical path variation due to vibrations of optical elements, air currents in the path of the beams, and the finite full width at half maximum (FWHM = 158 ± 12 Hz) of the RF signal applied to the AOM that prepares the reference beam. We found the FWHM of the master-slave beatnote (183 ± 34 Hz) to be consistent with a master-master beatnote (172 ± 25 Hz) within the error bars. The measurement indicated the spectral purity of the injected slave to be indistinguishable from that of the master. We also recorded a beatnote spectrum with a higher resolution bandwidth (100 kHz) over a span of 50 MHz to compare the noise floor of the slave laser with the master as shown in the right panel of Fig. 5. The noise floor with 12 mW of injected power achieves the same performance as the master, while with a smaller injection power, an increase in the noise floor is barely observable.

Absorption spectroscopy: to exclude the possible presence of higher frequency components in the slave emission beyond the photodetector bandwidth (1.2 GHz), we investigate the absorption spectra of a Sr atomic beam recorded with the master and the injected slave lasers independently. A collimated beam of atoms is generated from a strontium oven [59]. The oven contains a Sr reservoir terminated by a nozzle (diameter 4 mm, length 8 mm), filled with 8 mm long and 200 μm wide, 120 stainless steel capillaries. The oven is hosted in a vacuum system and maintained at an

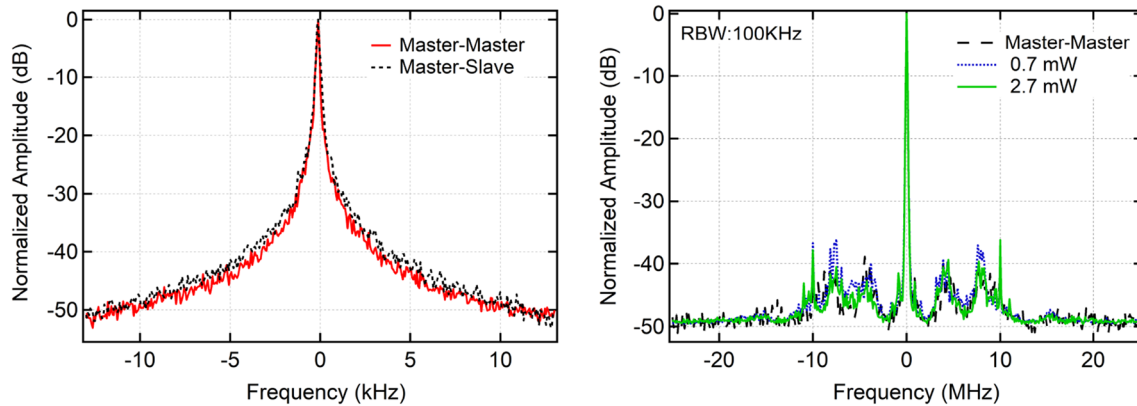


Fig. 5 Comparison of the spectral properties of the master and the slave lasers through a beatnote measurement. Left panel: beatnote of the reference beam with the injected slave (dashed black curve) and the master laser (solid red curve). The spectrum was recorded with a resolution bandwidth of 10 Hz over a span of 30 kHz. Right panel: beatnote with a higher resolution bandwidth (100 kHz) over a larger

frequency span (50 MHz) to compare the spontaneous (background) emission of the diode at different seed power. The plot indicates that the slave beam (solid green trace) reflects the same spectral properties as the master (dashed black trace) laser without adding significant phase noise. The noise level is slightly higher with lower injection power, as shown by the dotted blue trace

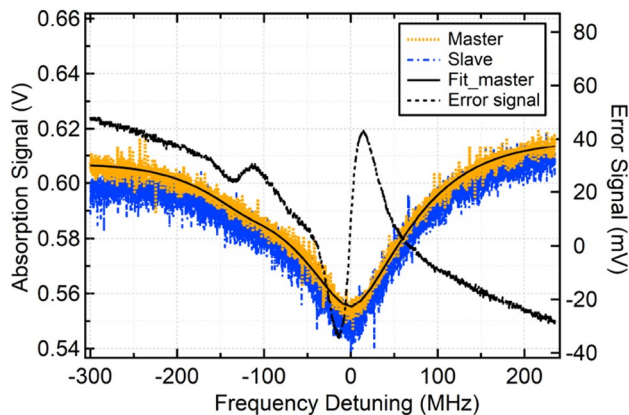


Fig. 6 Absorption spectroscopy measurement. The single-pass absorption spectrum of atoms probed with the master laser (dotted orange line) and slave laser (dashed-dotted blue line) as a function of detuning to the $^1S_0 - ^1P_1$ transition. An error signal (dashed black curve) from servo 1 is used to calibrate the time axis of the scan. The saturated absorption spectra recorded at $30 \mu\text{W}$ of probe powers with the master laser and the injection-locked slave laser are found to be in coincidence with each other within 6%. The solid black curve shows the fit to the absorption spectrum for the master laser

equilibrium pressure of 10^{-8} mbar when operated at 450°C . A linearly polarized probe beam of nearly $250 \mu\text{m}$ waist is aligned orthogonal to the atomic beam. The frequency of the probe beam is varied around the $^1S_0 - ^1P_1$ resonance, the absorption of the probe beam by the atomic beam is captured on a photodetector. Given the known isotope shift of ^{88}Sr and ^{86}Sr , an error signal (dashed black trace in Fig. 6) from servo 1 is used to calibrate the time axis of the oscilloscope. Figure 6 shows the spectra obtained with master laser and injected slave at $30 \mu\text{W}$ of incident probe power. For the

given level of probe power, the beam's intensity remains below the saturation intensity of the transition, thus avoiding the power broadening of the transition. The absorption spectrum is given by a convolution of the transverse velocity distribution and the natural Lorentzian profile. We observe that for a given power, the absorption profile observed with the master and the slave laser overlap with each other, indicating the spectral purity of the slave beyond the bandwidth of the photodetector. Indeed, if the slave laser had emission at wavelengths other than the master, the spectrum observed with the slave laser would have exhibited a large offset and a lower absorption peak. The offset would have been caused by a constant significant background of transmitted light and a lower absorption peak due to low power at the desired frequency.

To quantify our statement, we fit the observed data with the sum of two distributions corresponding to ^{88}Sr and ^{86}Sr (see appendix A) atoms. The fit to the data (absorption by the master) is shown in Fig. 6 as a solid black line. The relative peak absorption of the two spectra from the master and the slave are found to be in agreement with each other within 6%, confirming the spectral purity of the slave beyond the GHz range. The slave was operated at 300 mA and injected with 2.5 mW of power. The result confirms that the slave laser follows the master laser while keeping a single-mode emission, making the laser system tunable.

3.4 Intensity noise

To understand the optical power fluctuations of the slave, we investigated the relative intensity noise. We express the optical power of the laser as $P + \delta P(t)$ where P is the average power and δP is the fluctuating quantity with zero mean. The

relative intensity noise (RIN) can be expressed as δP divided by the average power, which is statistically described by a single-sided power spectral density (PSD), $S_{\text{RIN}}(f)$ as

$$S_{\text{RIN}}(f) = \frac{2}{P^2} \int \langle \delta P(t) \delta P(t + \tau) \rangle e^{-i2\pi f \tau} d\tau, \quad (3)$$

where f is the Fourier frequency. We measured the intensity noise directly with a silicon PIN photodiode (Hamamatsu S1223-01) mounted on a low-noise and high-gain transimpedance amplifier with a sensitivity of 2.61 mV/ μ W. This photodetector signal is fed to a spectrum analyzer (Agilent 35670A [51]) and, accounting for the average photodetector voltage, the spectrum of intensity fluctuations is computed.

Figure 7 shows the RIN of the injected and non-injected slave laser at two operating currents. The spectrum of the injected slave laser at the operating current of 296 mA shows a constant noise level of ≈ -124.5 dBc/Hz above 1 kHz. However, for the non-injected slave, the noise level is observed to be higher (≈ -118.9 dBc/Hz). It is also observed that the RIN of the slave laser decreases when operated at higher current. The background noise of the detector is measured to be < -149 dBc/Hz. A relative shot noise level can be calculated as $2h\nu/(QE \times P)$ where ν is the frequency of the laser and h is the Planck constant, QE, the quantum efficiency is 0.67 and the laser power $P = 383 \mu$ W. The RIN

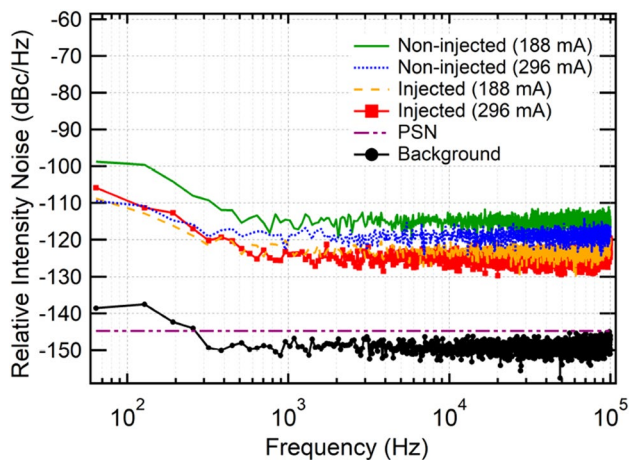


Fig. 7 Relative intensity noise of the slave at two different operating slave current with an injection power of 0.7 mW. The measured noise levels for the non-injected slave (green solid-line trace and blue dashed-line trace indicating slave operating current of 188 mA and 296 mA, respectively) are found to be higher than injected slave (orange dashed curve and square box-line indicating operating current of 188 mA and 296 mA, respectively). The Relative intensity noise of the slave decreases with higher operating current. The estimated relative photon shot noise (PSN) level and measured background noise floor without light are indicated by the purple double-dashed and dot-line black trace, respectively

levels of the injected slave are competitive with the levels achievable in frequency-doubled laser system.

4 Application of the laser system: magneto-optical trap

After investigating the spectral purity, tunability, and intensity noise of the injected slave, we used the laser system to implement a magneto-optical trap (MOT) for ^{88}Sr atoms. This would place the ultimate bar on the performance of the laser system as a laser source's relative intensity noise and frequency fluctuations are directly related to the trapped atom number fluctuations and temperature of the MOT. This section describes the experimental sequence to realize the MOT on the $^1S_0-^1P_1$ transition of strontium and its characterization. The vacuum system is composed of a compact atomic oven [59], an atomic beam shutter followed by a CF35 cube for transverse cooling, a bellow, an inline valve to stop the atomic beam flux without turning the oven off, a differential pumping tube, a Zeeman slower followed by an octagon science chamber, a CF63 four-way cross, two vacuum pumps, and the supporting parts. To maintain vacuum levels of 10^{-8} mbar in the oven side region, a 55 L/s ion pump (Agilent) is used. A vacuum level below 10^{-10} mbar in the science chamber is maintained by an ion-getter combination pump (Saes NEX Torr D500-5 [51]). When the oven is operated at a temperature of 450 °C, it emits an atomic beam of Sr atoms with a divergence of ≈ 70 mrad and most probable velocity of $v \approx 450$ m/s. These atoms are decelerated to ≈ 50 m/s in a 30 cm long tapered solenoid by a counter-propagating Zeeman slower beam. The Zeeman slower beam is red detuned by 481 MHz from the resonance and uses 33 mW of optical power. Slowed atoms are collected by the MOT, formed by a pair of anti-Helmholtz coils and three pairs of circularly polarized counter-propagating laser beams. One of the laser beams is aligned along the axis of the anti-Helmholtz coil and the other two beams are aligned orthogonal to each other and to the axial beam. A total of 22 mW of power is used to prepare these three pairs of MOT beams. Each beam typically has $1/e^2$ radius of 5 mm with 4 mW of power in the axial beam and 6 mW each in the other two beams. The total intensity at the location of the atoms is estimated to be 81.5 mW/cm². At the center of the MOT chamber, a magnetic field gradient close to 45 G/cm is applied. About 2 mW of repumper beam at 497 nm, generated by frequency doubling an amplified 994 nm ECDL laser, are superimposed with one of the MOT beams to recycle the atoms lost to the 3P_2 metastable state [60, 61]. We characterize the loading of the blue MOT by collecting the fluorescence on a high-gain photodetector as shown in Fig. 8.

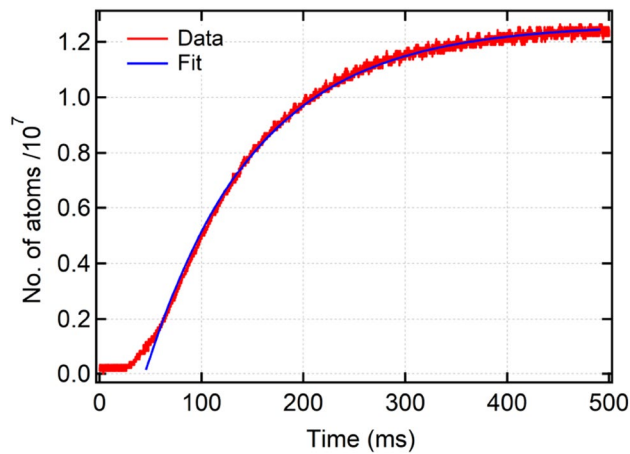


Fig. 8 ^{88}Sr MOT loading curve. The figure shows the number of atoms collected in the MOT as a function of time. The Zeeman slower beam, MOT beams and the repumper at 497 nm were kept continuously on the rise. The data (red trace) are fitted with the empirical equation $N(t) = R\tau(1 - e^{-t/\tau})$ (blue trace), where R is the MOT loading rate and τ^{-1} is the loss rate. The typical MOT loading time and rate are estimated to be 106.6 ms and 1.2×10^8 atoms/s

The loading curve can be fitted with an empirical equation $N(t) = R\tau(1 - e^{-t/\tau})$, where R is the MOT loading rate and τ^{-1} is the loss rate from the MOT. The results show that the typical MOT loading time τ is 106.6 ms, and the MOT loading rate R is 1.2×10^8 atoms/sec. We further characterize the MOT temperature with the standard time-of-flight (TOF) method. The atoms are loaded into the MOT for ≈ 1 s. After this, MOT beams and magnetic fields are turned off, and an on-resonance probe pulse of $50 \mu\text{s}$ is applied to capture the absorption image on a CCD camera. After a wait time of 30 ms, another probe pulse is sent to capture a reference image. A typical absorption image of the MOT is shown in the inset of Fig. 9a. The number of atoms computed from the absorption images is found to be 1.4×10^7 . For the blue MOT, a TOF measurement of up to 3 ms can be performed with a sufficient signal-to-noise ratio for a temperature measurement. The horizontal width of the cloud, derived by fitting the row sum of the image, is shown in Fig. 9a as a function of the time of flight. The evolution of the width of the thermal cloud is given as

$$\sigma_x^2(t) = \sigma_x^2(0) + \frac{k_B T t^2}{m}, \quad (4)$$

where σ_x is the Gaussian width of the cloud, T is the temperature of the cloud, and m is the atomic mass. Using this

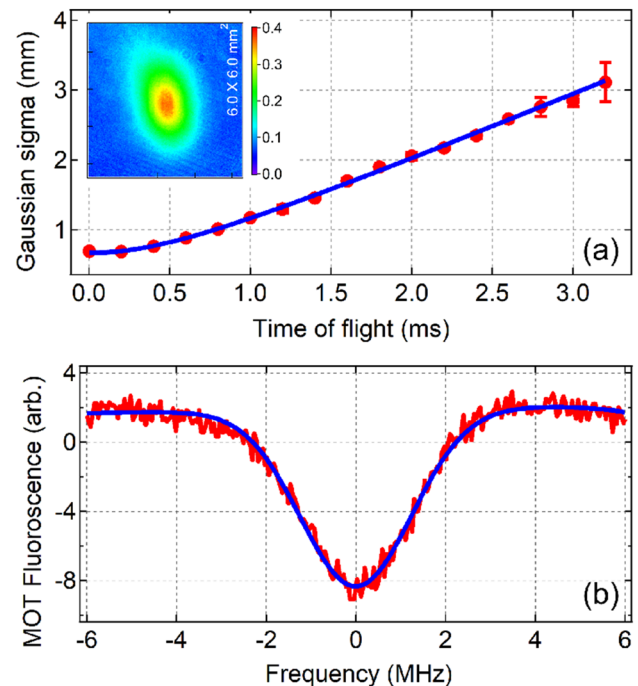


Fig. 9 Temperature measurement of atoms in the MOT. Plot (a) shows the Gaussian width (red-filled circles) of the atomic cloud as a function of free fall time. The inset is the typical absorption image of the atomic cloud recorded with TOF= 400 μs , the color scale shows the optical density. The temperature estimated from the TOF measurement is found to be 9.7 ± 1.3 mK. Plot (b) shows the blue MOT fluorescence signal as a function of the 689 nm laser detuning from the resonance of the $^1\text{S}_0(m=0) \rightarrow ^3\text{P}_1(m=0)$ transition. The temperature of the corresponding free atomic cloud is estimated to be 11.1 ± 1.4 mK from the width of this spectrum. The solid blue curve is a Gaussian fit to the experimental data

TOF measurement, we estimate the MOT temperature to be 9.7 ± 1.3 mK.

Due to a relatively large cloud size and high velocities of the atoms, the conventional method to optimize the MOT by monitoring the expansion of the cloud is not sensitive enough, and an alternative method as described in Ref. [62] can be adapted for the optimization. This method is based on illuminating a continuously-running MOT with 689 nm laser light, close to the resonance of the 7.5 kHz linewidth $^1\text{S}_0 \rightarrow ^3\text{P}_1$ transition. The population transfer to the $^3\text{P}_1$ state results in a frequency-dependent depletion of the MOT fluorescence signal that can be used to determine the cloud temperature. A typical spectrum, corresponding to the Doppler-sensitive $^1\text{S}_0(m=0) \rightarrow ^3\text{P}_1(m=0)$ transition can be seen in Fig. 9b. Excitation to the $m = \pm 1$ states is strongly affected by the MOT's inhomogeneous field profile and therefore has to be discarded in this temperature

measurement. The atoms were illuminated with an intensity of $462 I_{\text{sat}}$, where $I_{\text{sat}} = 3 \mu\text{W}/\text{cm}^2$ is the saturation intensity of the $^1\text{S}_0\text{-}^3\text{P}_1$ transition. This results in a power-broadened linewidth of 160 kHz corresponding to a 0.1 m/s velocity resolution. The measured Gaussian width of the fluorescence dip is $\delta\nu = 1.05$ MHz. Accounting for the fact that the velocity distribution here is measured for trapped atoms and using the equipartition theorem, the temperature of the corresponding free cloud can be estimated as $T = 2mv_{\text{rms}}^2/k_B$. Here m is the atomic mass and v_{rms} is the root-mean-square velocity of the trapped cloud, given by the Doppler shift as $\lambda\delta\nu$, with $\lambda = 689.45$ nm, the wavelength of the $^1\text{S}_0(m=0)\text{-}^3\text{P}_1(m=0)$ transition. This measurement yields a temperature $T = 11.1 \pm 1.4$ mK, consistent within one standard deviation with the TOF measurement.

By monitoring the absorption signal and relative amplitude of the side peaks, optimization of the MOT can be performed with respect to intensity, alignment, polarization, and detuning of the MOT beams. We aligned the MOT position with the magnetic field zero to achieve a symmetric and low-temperature atomic cloud. The temperature of the achieved MOT agrees with previously reported results and we thus conclude that the laser system is suitable for strontium precooling.

5 Conclusion

In conclusion, we have demonstrated a simple, scalable, tunable master-slave injection-locked laser system capable of generating 500 mW at 460.86 nm with a narrow linewidth of $\simeq 1.6$ MHz and frequency tunability of 1.4 GHz. We carried out a detailed characterization of the laser system and implemented a simple active injection stabilization scheme. The laser system characterized via various measurements establishes the spectral purity of the injection-locked slave laser to be indistinguishable from that of the master. The relative intensity noise of the laser system was found to be competitive with typical frequency-doubled laser systems. The reported laser configuration consumes less than 100 W of electrical power with a room for improvement, making it a possible choice for space-borne experiments. We realized the first stage cooling and trapping of Sr atoms using the reported laser system. The reported laser system can guide in designing similar high-power laser sources at other wavelengths using appropriate master and slave diodes. For example, adapting this setup to the production of cold ytterbium samples using the recently launched high power laser diode (Nichia NDV4B16 [46, 51]) operated at 399 nm, appears straightforward with current technology. The laser system offers a prominent alternative to the existing frequency-doubled laser systems in terms of cost, design flexibility, electrical power consumption, ease of scaling, intensity stability,

and frequency tunability. Over a period of one year, we see no significant aging effect on our system, predicting a ~ 5 year lifetime of our system.

Appendix A

Absorption spectroscopy

As reported in Ref. [63], due to the confinement from the capillaries, the velocity distribution of the thermal atomic beam can be represented as the probability density function

$$P(v, a) = \frac{|v| \exp(-v^2/v_0^2) \Gamma(-1/2, v^2\alpha/v_0^2)}{2\sqrt{\pi/\alpha} (\sqrt{\alpha+1} - \sqrt{\alpha}) v_0^2}, \quad (5)$$

where $\alpha = L^2/a^2$, $v_0 = \sqrt{3k_B T/m}$ is the most probable velocity, L and a are the length and diameter of the capillaries, respectively and $\Gamma(-1/2, v^2 L^2/v_0^2 a^2)$ is the incomplete gamma function.

We can then compute the expected absorption signal for a probe beam propagating orthogonal to the atomic beam direction. We use Beer's law for the ratio I_t/I_0 of transmitted to incident intensity,

$$\frac{I_t}{I_0} = e^{-n\sigma} \simeq 1 - n\sigma, \quad (6)$$

where $n(x, y)$ is the 2D atom density in a plane perpendicular to the probe beam (propagating along z) and $\sigma = \sigma_0/(1 + I_0/I_{\text{sat}} + 4\Delta^2/\Gamma^2)$ is the absorption cross section, with $\sigma_0 = 3\lambda^2/2\pi$ and Δ is the detuning of the probe beam from resonance. The transmitted power of the probe beam is related to the transmitted intensity as $P_t = \int I_t(x, y) dx dy$. Using Eq. 6, the transmitted power can be written as

$$P_t = \int dx dy I_0(x, y) \left[1 - \int n'(x, y, v_z) \sigma(\Delta - kv_z) dv_z \right]. \quad (7)$$

In this expression, $n'(x, y, v_z)$ is the number of atoms per area element $dx dy$ per velocity element dv_z . We make the assumption that, in the density, the x and y coordinates are independent of the velocity v_z in the probe propagation direction. This is indeed generally true since a velocity v_z will map into a position z but will not change x and y . As a result, we can write $n'(x, y, v_z) = n(x, y) n_v(v_z)$ where $n_v(v_z)$ is the number of atoms per unit velocity. Thus transmitted power can be expressed as

$$P_t = P_0 - \int dx dy n(x, y) I_0(x, y) \int n_v(v_z) \sigma(\Delta - kv_z) dv_z, \quad (8)$$

here, $n_v(v_z)$ is proportional to the velocity distribution of the atomic beam. This leads to an expression of the form

$$P_0 - P_t = A \int P(v, a) \sigma(\Delta - kv_z) dv_z. \quad (9)$$

This equation represents the inverted absorption profile of the atoms as a function of atomic velocity with a peak amplitude A . The observed absorption spectroscopy signal as shown in Fig. 6 can be fitted with the sum of two such distributions corresponding to contributions from ^{88}Sr and ^{86}Sr atoms. The signal is fitted, keeping the amplitude of the two absorption peaks, the resonant frequency of ^{88}Sr absorption peak, α and a linear baseline of the signal as free parameters. To establish the spectral purity of the slave laser, we compare the absorption spectra obtained when probed with the master and the slave respectively. A good comparison is given by the amplitudes of the two signals. If A_m and A_s are the amplitudes of the ^{88}Sr absorption peak for the master and the slave laser respectively and y_m and y_s are the corresponding offsets (indicating the incident power) as obtained by the fitting, then two lasers have the same spectrum if $A_m/y_m = A_s/y_s$. If we call $r_m = A_m/y_m$ and $r_s = A_s/y_s$, then the fractional coincidence between the two spectra can be defined as $|r_m - r_s| / ((r_m + r_s)/2)$ i.e. the difference in the absorption ratio normalized by the average value. The two spectra agree within 6 %.

Acknowledgements We acknowledge financial support from INFN under the project OLAGS. GV, EW, and GR acknowledge support from MIUR (Italian Ministry of Education, Universities and Research) under the FARE-TENMA project. GV acknowledges support from the project QuEGI-Quantum Enhanced Gravity Interferometry of Università di Firenze. JA acknowledges support from ESA under contract number 4000129848/20/NL/MH/ac. LS and NP acknowledges support from the European Research Council, Grant No. 772126 (TICTOCGRAV). NP acknowledges financial support from European Unions Horizon 2020 Programme, under the project TAIOL of QuantERA ERA-NET Cofund in Quantum Technologies (Grant Agreement No. 731473).

Funding Open access funding provided by Università degli Studi di Firenze within the CRUI-CARE Agreement.

Open Access This article is licensed under a Creative Commons Attribution 4.0 International License, which permits use, sharing, adaptation, distribution and reproduction in any medium or format, as long as you give appropriate credit to the original author(s) and the source, provide a link to the Creative Commons licence, and indicate if changes were made. The images or other third party material in this article are included in the article's Creative Commons licence, unless indicated otherwise in a credit line to the material. If material is not included in the article's Creative Commons licence and your intended use is not permitted by statutory regulation or exceeds the permitted use, you will need to obtain permission directly from the copyright holder. To view a copy of this licence, visit <http://creativecommons.org/licenses/by/4.0/>.

References

1. Q. Luo, H. Zhang, K. Zhang, X.C. Duan, Z.K. Hu, L.L. Chen, M.K. Zhou, *Rev. Sci. Instrum.* (2019). <https://doi.org/10.1063/1.5053132>
2. O. Carraz, F. Lienhart, R. Charrière, M. Cadoret, N. Zahzam, Y. Bidet, A. Bresson, *Appl. Phys. B* **97**, 405 (2009). <https://doi.org/10.1007/s00340-009-3675-9>
3. A.D. Ludlow, M.M. Boyd, J. Ye, E. Peik, P.O. Schmidt, *Rev. Mod. Phys.* **87**, 637 (2015). <https://doi.org/10.1103/RevModPhys.87.637>
4. G.M. Tino, M.A. Kasevich, *Atom Interferometry: Proceedings of the International School of Physics "Enrico Fermi", Course 188, Varenna on Lake Como, Villa Monastero, 15-20 July 2013*. International School of Physics Enrico Fermi Series (IOS Press, 2014). <https://books.google.co.in/books?id=OV7IrQEACAAJ>
5. G. Rosi, F. Sorrentino, L. Cacciapuoti, M. Prevedelli, G.M. Tino, *Nature* **510**, 518 (2014). <https://doi.org/10.1038/nature13433>
6. I. Dutta, D. Savoie, B. Fang, B. Venon, C.L. Garrido Alzar, R. Geiger, A. Landragin, *Phys. Rev. Lett.* **116**, 183003 (2016). <https://doi.org/10.1103/PhysRevLett.116.183003>
7. F. Schäfer, T. Fukuhara, S. Sugawa, Y. Takasu, Y. Takahashi, *Phys. Rev. Phys.* **2**, 411 (2020). <https://doi.org/10.1038/s42254-020-0195-3>
8. U.D. Rapol, A. Krishna, A. Wasan, V. Natarajan, *Eur. Phys. J. D-At. Mol. Opt. Plasm. Phys.* **29**, 409 (2004). <https://doi.org/10.1140/epjd/e2004-00041-3>
9. N. Hinkley, J.A. Sherman, N.B. Phillips, M. Schioppo, N.D. Lemke, K. Beloy, M. Pizzocaro, C.W. Oates, A.D. Ludlow, *Science* **341**(6151), 1215 (2013). <https://doi.org/10.1126/science.1240420>
10. C. Degenhardt, H. Stoehr, U. Sterr, F. Riehle, C. Lisdat, *Phys. Rev. A* **70**, 023414 (2004). <https://doi.org/10.1103/PhysRevA.70.023414>
11. G. Ferrari, P. Cancio, R. Drullinger, G. Giusfredi, N. Poli, M. Prevedelli, C. Toninelli, G.M. Tino, *Phys. Rev. Lett.* **91**, 243002 (2003). <https://doi.org/10.1103/PhysRevLett.91.243002>
12. J.J. McFerran, L. Yi, S. Mejri, S. Di Manno, W. Zhang, J. Guéna, Y. Le Coq, S. Bize, *Phys. Rev. Lett.* **108**, 183004 (2012). <https://doi.org/10.1103/PhysRevLett.108.183004>
13. O.N. Prudnikov, D.V. Brazhnikov, A.V. Taichenachev, V.I. Yudin, A.E. Bonert, R.Y. Il'envkov, A.N. Goncharov, *Phys. Rev. A* **92**, 063413 (2015). <https://doi.org/10.1103/PhysRevA.92.063413>
14. J.N. Tinsley, S. Bandarupally, J.P. Penttinen, S. Manzoor, S. Ranta, L. Salvi, M. Guina, N. Poli, *Opt. Express* **29**(16), 25462 (2021). <http://www.opticsexpress.org/abstract.cfm?URI=oe-29-16-25462>
15. S. Stellmer, B. Pasquiou, R. Grimm, F. Schreck, *Phys. Rev. Lett.* **110**, 263003 (2013). <https://doi.org/10.1103/PhysRevLett.110.263003>
16. G.E. Marti, R.B. Hutson, A. Goban, S.L. Campbell, N. Poli, J. Ye, *Phys. Rev. Lett.* **120**, 103201 (2018). <https://doi.org/10.1103/PhysRevLett.120.103201>
17. W.F. McGrew, X. Zhang, R.J. Fasano, S.A. Schäffer, D. Beloy, K. Nicolodi, R.C. Brown, N. Hinkley, G. Milani, M. Schioppo, T.H. Yoon, A.D. Ludlow, *Nature* **564**, 87 (2018). <https://doi.org/10.1038/s41586-018-0738-2>
18. S.L. Campbell, R.B. Hutson, G.E. Marti et al., *Science* **358**(6359), 90 (2017). <https://doi.org/10.1126/science.aam5538>
19. L. Hu, N. Poli, L. Salvi, G.M. Tino, *Phys. Rev. Lett.* **119**, 263601 (2017). <https://doi.org/10.1103/PhysRevLett.119.263601>
20. G.M. Tino, *Quantum Sci. Technol.* (2021). <https://doi.org/10.1088/2058-9565/abd83e>

21. B. Canuel, S. Abend, P. Amaro-Seoane et al., *Class. Quantum Gravity* (2020). <https://doi.org/10.1088/1361-6382/aba80e>
22. L. Badurina, E. Bentine, D. Blas, K. Bongs et al., *J. Cosmol. Astropart. Phys.* **2020**(05), 011 (2020). <https://doi.org/10.1088/1475-7516/2020/05/011>
23. P. Adamson, S. Chattopadhyay, J. Coleman et al., (2018). <https://www.osti.gov/biblio/1605586>
24. G.M. Tino, A. Bassi, G. Bianco et al., *Eur. Phys. J. D* **73**(11), 228 (2019). <https://doi.org/10.1140/epjd/e2019-100324-6>
25. Y.A. El-Neaj, C. Alpigiani, S. Amairi-Pyka et al., *EPJ Quantum Technol.* (2020). <https://doi.org/10.1140/epjqt/s40507-020-0080-0>
26. D. Becker, M.D. Lachmann, S.T. Seidel et al., *Nature* **562**, 391 (2018). <https://doi.org/10.1038/s41586-018-0605-1>
27. M.G. Tarallo, T. Mazzoni, N. Poli, D.V. Sutyryn, X. Zhang, G.M. Tino, *Phys. Rev. Lett.* **113**, 023005 (2014). <https://doi.org/10.1103/PhysRevLett.113.023005>
28. M.A. Hohensee, H. Müller, R.B. Wiringa, *Phys. Rev. Lett.* **111**, 151102 (2013). <https://doi.org/10.1103/PhysRevLett.111.151102>
29. T. Damour, *Class. Quantum Gravity* (2012). <https://doi.org/10.1088/0264-9381/29/18/184001>
30. T. Akatsuka, K. Hashiguchi, T. Takahashi, N. Ohmae, M. Takamoto, H. Katori, *Phys. Rev. A* **103**, 023331 (2021). <https://doi.org/10.1103/PhysRevA.103.023331>
31. A. Sitaram, P.K. Elgee, G.K. Campbell, N.N. Klimov, S. Eckel, D.S. Barker, *Rev. Sci. Instrum.* (2020). <https://doi.org/10.1063/5.0019551>
32. J.I. Kim, D. Haubrich, D. Meschede, *Opt. Express* **17**(23), 21216 (2009). <http://www.opticsexpress.org/abstract.cfm?URI=oe-17-23-21216>
33. F. Mühlbauer, N. Petersen, C. Baumgärtner, L. Maske, P. Windpassinger, *Appl. Phys. B* **124**, 120 (2018). <https://doi.org/10.1007/s00340-018-6981-2>
34. H.Y. Ban, M. Jacka, J.L. Hanssen, J. Reader, J.J. McClelland, *Opt. Express* **13**(8), 3185 (2005). <http://www.opticsexpress.org/abstract.cfm?URI=oe-13-8-3185>
35. Y. Kaneda, J.M. Yarborough, Y. Merzlyak, A. Yamaguchi, K. Hayashida, N. Ohmae, H. Katori, *Opt. Lett.* **41**(4), 705 (2016). <http://ol.osa.org/abstract.cfm?URI=ol-41-4-705>
36. M. de Angelis, G.M. Tino, P.D. Natale, C. Fort, G. Modugno, M. Prevedelli, C. Zimmermann, *Appl. Phys. B* **62**, 333 (1996)
37. G. Verma, C. Vishwakarma, C.V. Dharmadhikari, U.D. Rapol, *Rev. Sci. Instrum.* (2017). <https://doi.org/10.1063/1.4977593>
38. B. Boulanger, M.M. Fejer, R. Blachman, P.F. Bordui, *Appl. Phys. Lett.* **65**(19), 2401 (1994). <https://doi.org/10.1063/1.112688>
39. J. Villarroel, J. Carnicero, F. Luedtke, M. Carrascosa, A.G.C. nes, J.M. Cabrera, A. Alcazar, B. Ramiro, *Opt. Express* **18**(20), 20852 (2010). <http://www.opticsexpress.org/abstract.cfm?URI=oe-18-20-20852>
40. C.H. Feng, S. Vidal, P. Robert, P. Bouyer, B. Desruelle, M. Prevedelli, J. Boulet, G. Santarelli, A. Bertoldi, *Opt. Express* **29**(17), 27760 (2021). <http://www.opticsexpress.org/abstract.cfm?URI=oe-29-17-27760>
41. V.M. Schäfer, C.J. Ballance, C.J. Tock, D.M. Lucas, *Opt. Lett.* **40**(18), 4265 (2015). <http://ol.osa.org/abstract.cfm?URI=ol-40-18-4265>
42. S.P. Najda, P. Perlin, T. Suski, L. Marona, S. Stanczyk, P. Wisniewski, R. Czerniecki, D. Schiavon, M. Leszczyński, in *Gallium Nitride Materials and Devices XIII*, ed. by J.I. Chyi, H. Fujioka, H. Morkoç. International Society for Optics and Photonics (SPIE, 2018), vol. 10532, pp. 72 – 78. <https://doi.org/10.1117/12.2286044>
43. S. Stanczyk, A. Kafar, S. Grzanka, M. Sarzynski, R. Mroczynski, S. Najda, T. Suski, P. Perlin, *Opt. Express* **26**(6), 7351 (2018). <http://www.opticsexpress.org/abstract.cfm?URI=oe-26-6-7351>
44. G. Hadley, *IEEE J. Quantum Electron.* **22**(3), 419 (1986). <https://doi.org/10.1109/JQE.1986.1072979>
45. V. Schkolnik, J.R. Williams, N. Yu. Generating 500 mW for laser cooling of strontium atoms by injection locking a high power laser diode (2020). <https://arxiv.org/abs/2004.11732v1>
46. T. Hosoya, M. Miranda, R. Inoue, M. Kozuma, *Rev. Sci. Instrum.* (2015). <https://doi.org/10.1063/1.4927132>
47. F. Yuan, *Injection-locking of oscillators: an overview* (Springer International Publishing, Cham, 2020), pp. 1–23. https://doi.org/10.1007/978-3-030-17364-7_1
48. W. Chow, *IEEE J. Quantum Electron.* **19**(2), 243 (1983). <https://ieeexplore.ieee.org/document/1071829>
49. C.J.H. Pagett, P.H. Moriya, R. Celistrino Teixeira, R.F. Shiozaki, M. Hemmerling, P.W. Courteille, *Rev. Sci. Instrum.* **87**(5), 053105 (2016). <https://doi.org/10.1063/1.4947462>
50. B. Saxberg, B. Plotkin-Swing, S. Gupta, *Rev. Sci. Instrum.* (2016). <https://doi.org/10.1063/1.4953589>
51. Citing part numbers does not imply endorsement by the host institutions
52. R.G. Escudero, C.C. Chen, S. Bennetts, B. Pasquiou, F. Schreck, *Phys. Rev. Res.* **3**, 033159 (2021). <https://doi.org/10.1103/PhysRevResearch.3.033159>
53. K.S. Hardman, S. Bennetts, J.E. Debs, C.C.N. Kuhn, G.D. McDonald, N. Robins, *JoVE* **86**, e51184 (2014). <https://doi.org/10.3791/51184>
54. B. Bloom, Building a better atomic clock. Ph.D. thesis, Boulder (2014). <https://jila.colorado.edu/bibcite/reference/3362>
55. M.K. Shaffer, G. Ranjit, C.I. Sukenik, *Rev. Sci. Instrum.* (2008). <https://doi.org/10.1063/1.2906224>
56. G.D. Domenico, S. Schilt, P. Thomann, *Appl. Opt.* **49**(25), 4801 (2010). <http://ao.osa.org/abstract.cfm?URI=ao-49-25-4801>
57. Z. Liu, R. Slavík, J. ghtwave Technol. **38**(1), 43 (2020). <http://www.osapublishing.org/jlt/abstract.cfm?URI=jlt-38-1-43>
58. O.J. Hao. Active stabilization of an injection lock (BSc thesis, National University of Singapore, 2019). <https://www.physics.nus.edu.sg/wp-content/uploads/sites/5/2020/08/hyp-1819-13.pdf>
59. M. Schioppo, N. Poli, M. Prevedelli, S. Falke, C. Lisdat, U. Sterr, G.M. Tino, *Rev. Sci. Instrum.* (2012). <https://doi.org/10.1063/1.4756936>
60. S. Stellmer, F. Schreck, *Phys. Rev. A* **90**, 022512 (2014). <https://doi.org/10.1103/PhysRevA.90.022512>
61. N. Poli, R.E. Drullinger, G. Ferrari, J. Léonard, F. Sorrentino, G.M. Tino, *Phys. Rev. A* **71**, 061403 (2005). <https://doi.org/10.1103/PhysRevA.71.061403>
62. K.Y. Khabarova, A.A. Galyshev, S.A. Strelkin, A.S. Kostin, G.S. Belotelov, O.I. Berdasov, A. Gribov, N.N. Kolachevsky, S.N. Slyusarev, *Quantum Electron.* **45**(2), 166 (2015). <https://doi.org/10.1070/qe2015v045n02abeh015638>
63. F. Gao, H. Liu, P. Xu, X. Tian, Y. Wang, J. Ren, H. Wu, H. Chang, *AIP Adv.* (2014). <https://doi.org/10.1063/1.4866983>

Publisher's Note Springer Nature remains neutral with regard to jurisdictional claims in published maps and institutional affiliations.